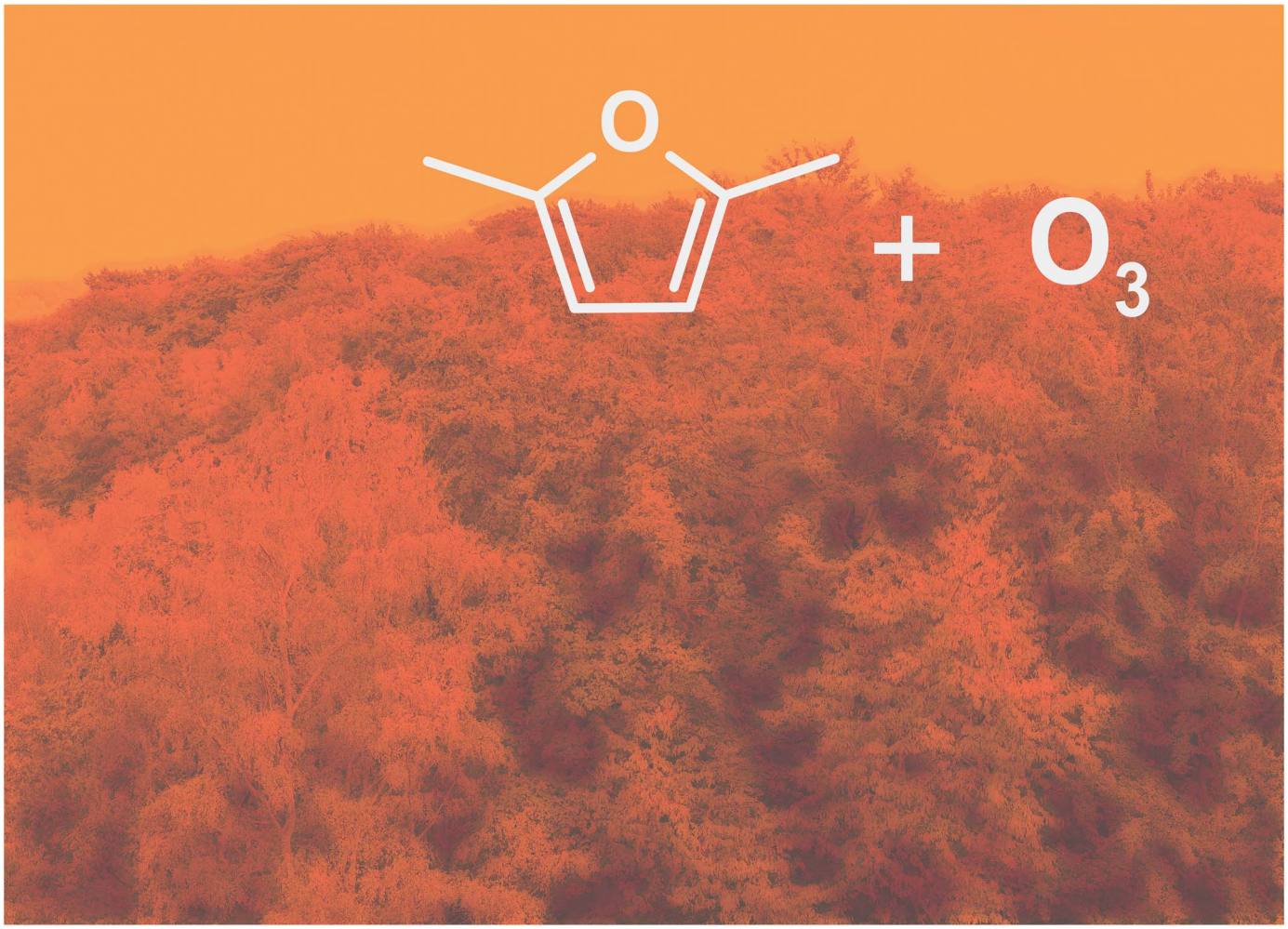

Showcasing research from the Institute for Atmospheric and Environmental Research, University of Wuppertal, Germany.

O_3 chemistry of 2,5-dimethylfuran: mechanism development

The gas-phase ozonolysis of 2,5-dimethylfuran was investigated in a quartz glass atmospheric simulation chamber. 2,5-Dimethylfuran was found to be highly reactive towards O_3. The target reaction produces a range of small reactive species as well as compounds contributing to atmospheric acidity like acetic acid and acetic anhydride.

As featured in:

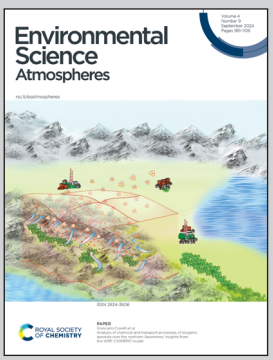

See Niklas Illmann and Vera Rösgen, *Environ. Sci.: Atmos.*, 2024, **4**, 1000.

ROYAL SOCIETY OF CHEMISTRY

rsc.li/esatmospheres

Registered charity number: 207890

Environmental Science: Atmospheres

ROYAL SOCIETY OF CHEMISTRY

PAPER

View Article Online
View Journal | View Issue

Open Access Article. Published on 19 8 2024. Downloaded on 2026/02/16 5:19:08.
This article is licensed under a Creative Commons Attribution 3.0 Unported Licence.

Check for updates

Cite this: *Environ. Sci.: Atmos.*, 2024, **4**, 1000

O_3 chemistry of 2,5-dimethylfuran: mechanism development†

Niklas Illmann * and Vera Rösgen

Received 10th April 2024
Accepted 13th August 2024

DOI: 10.1039/d4ea00045e

rsc.li/esatmospheres

Furans are emitted from biomass burning (BB) and contribute to the reactivity of BB plumes with a significant proportion. Consequently, the development of comprehensive furan oxidation schemes is one of the crucial elements towards a better understanding of BB plume chemistry. Nighttime oxidation is supposedly dominated by NO_3 radicals and O_3. The present study has chosen 2,5-dimethylfuran (25DMF) as a model compound for the development of an O_3 oxidation mechanism for furans. Experiments were performed in the QUAREC atmospheric simulation chamber (QUAREC ASC) at 299 ± 2 K and a pressure of 980 ± 20 mbar under dry conditions (relative humidity < 0.1%) targeting the reaction kinetics, the OH formation and the oxidation mechanism. The reactions were monitored by long-path FTIR spectroscopy and a PTR-ToF-MS instrument. We determined a rate coefficient of (3.3 ± 1.0) × 10^{-16} cm^3 $molecule^{-1}$ s^{-1} for the target reaction using the relative-rate method. An OH yield of 25 ± 10% was obtained when using 1,3,5-trimethylbenzene as an OH tracer. Reaction products are formaldehyde, methyl glyoxal, ketene, glyoxal, methyl hydroperoxide, acetic anhydride, and acetic acid, respectively. The methyl glyoxal, glyoxal and formaldehyde yields were found to be sensitive to the overall peroxy radical level in the system. The PTR-MS data indicate further reaction products, which are tentatively assigned. A mechanism is postulated to account for the clearly identified reaction products. Overall, the obtained results indicate that O_3 oxidation of furans might contribute to acidity in nighttime BB plumes.

Environmental significance

Furan derivatives have been shown to represent major components of biomass burning (BB) smoke. To date, research on furan oxidation mechanisms is dominated by daytime chemistry. In this study we look into the nighttime oxidation of 2,5-dimethylfuran by O_3 to provide a basis for assessing the importance of O_3 chemistry on nighttime BB plumes. We were able to show that such reactions may contribute to the reactivity and acidity inside plumes. The results can be used for the development of a comprehensive O_3 oxidation scheme for furans to refine atmospheric models describing the ageing of nighttime BB plumes.

Introduction

Furan derivatives (furans, furaldehydes, furan alcohols *etc.*) are versatile chemicals of use in industry for various applications and (easily) accessible from lignocellulosic biomass (see Jaswal *et al.*[1] and references therein). 2,5-dimethylfuran (25DMF), in particular, raised interest as a biofuel candidate.[2] Furan derivatives arise from pyrolysis of cellulose which explains their presence in biomass burning (BB) smoke, particularly from wildfires.[3] For instance, furan derivatives accounted for up to 37% (by emission factor) of the smoke from different fuel types in laboratory studies.[4] In light of their high reactivity towards atmospheric oxidants, such as OH [5–7] and NO_3 [8] radicals, it is not surprising that furans contribute significantly to the total OH [9] and NO_3 [10] reactivity of wildfires characteristic emissions.

The chemistry inside BB plumes has been one of the major topics in atmospheric science during the last decade, primarily due to intensifying occurrence and magnitude of wildfire events.[11,12] A major scientific goal is the ability to predict ozone and particle formation (during plume ageing along the transport), which appears still challenging as a consequence of the multitude of possible chemical composition and reaction conditions inside plumes. Research on BB plume chemistry is still focused on the OH reactivity, since OH represents the predominant atmospheric oxidant on average and OH concentrations exceeding the typical tropospheric level by up to factor of 10 were found inside BB plumes for daytime conditions.[3,13]

More recently NO_3 chemistry has started to receive increasing attention.[10] However, O_3 initiated oxidation of unsaturated non-methane hydrocarbons (NMHC) is, to the best of our knowledge, not extensively addressed in discussions on

University of Wuppertal, Institute for Atmospheric and Environmental Research, Gaußstraße 20, 42119 Wuppertal, Germany. E-mail: illmann@uni-wuppertal.de

† Electronic supplementary information (ESI) available. See DOI: https://doi.org/10.1039/d4ea00045e

© 2024 The Author(s). Published by the Royal Society of Chemistry

Open Access Article. Published on 19 8 2024. Downloaded on 2026/02/16 5:19:08.
This article is licensed under a Creative Commons Attribution 3.0 Unported Licence.

BB plume chemistry with only very few exceptions. Decker *et al.*[10] found O_3 reactions to account for up to 43% of the nighttime NMHC oxidation in agricultural BB plumes based on box-model assisted analysis of aircraft observations. Yet, they stated their reactivity calculations were limited mainly by a lack of kinetic and mechanistic data.

Furans are heterocyclic aromatic species, whose aromaticity is much less pronounced than that of benzene. They can be regarded as cyclic ethers exhibiting reactivities close to conventional dienes *e.g.* in organic synthesis. Consequently, they are susceptible to ozonolysis reactions. Yet, at present information on the reactivity of furans towards ozone in the gas-phase is limited. Atkinson *et al.*[14] reported the first experimentally determined rate coefficient for the gas-phase ozonolysis of furan. Although the reactivity was found to be low and comparable to that ethene, this value did, however, confirm that furans, in general, are reactive towards ozone. Matsumoto[15] showed that rate coefficients are significantly larger for higher substituted furans such as 2,5-dimethylfuran, which was subsequently supported by a theoretical study on several furan derivatives.[16] Recently, the secondary organic aerosol formation from the 2,5-dimethylfuran ozonolysis was investigated and found to be negligible in the absence of SO_2.[17] Information on the ozonolysis mechanism of furans is, however, limited to one report on the OH production[18] and a single theoretical calculation.[16] No experimental data on reaction products were, to the best of our knowledge, ever reported in the literature.

Assessing the potential impact of O_3 chemistry on the nighttime chemical evolution of wildfire emissions requires a detailed knowledge of the ozonolysis kinetics and mechanisms of major plume constituents such as furans. The present study thus intends to serve as a basis for the development of a comprehensive furan ozonolysis mechanism by investigating the O_3 initiated oxidation of the symmetrical 2,5-dimethylfuran.

Experimental

Atmospheric simulation chamber (QUAREC ASC)

The experiments were performed in a cylindrical 1080 L quartz-glass atmospheric simulation chamber (QUAREC ASC) located at the University of Wuppertal. A white-type mirror system is installed inside the glass tube, which is coupled to a Fourier-transform infrared (FTIR) spectrometer and operated at an optical path length of 484.7 ± 0.8 m in total. The current set-up of the chamber is described in greater detail elsewhere.[19]

Experimental approach

All experiments were carried out under dry conditions (r. h. << 0.1%) at 980 ± 20 mbar of synthetic air (Messer, 99.9999%) and a temperature of 299 ± 2 K. A summary of the experimental conditions and initial concentrations is provided in Table S1 of the ESI† for all experiments. The ozonolysis reaction was initiated by adding O_3 to the reaction mixture (according to the experiment type), which was generated by passing a stream of pure oxygen (Messer, 99.995%) through an electrical discharge in a homemade device. Aliquots of (0.6–1.3) × 10^{13} cm^{-3} O_3 were added up to four times per experiment. The reaction mixtures were continuously stirred with all three fans mounted inside the chamber to keep the system as homogenous as possible. The mixtures were observed for about 7–30 min prior to adding O_3 to determine wall losses of target species in each single experiment. Three types of experiments were performed targeting the OH formation, the determination of the ozonolysis rate coefficient and the product formation, respectively. 1,3,5-Trimethylbenzene (Sigma-Aldrich, 99%) was added as a tracer to estimate the OH production. Carbon monoxide (Air Liquide, 99.97%) was added in excess (≈2%) to scavenge OH radicals in the experiments investigating the product formation and the kinetics. In addition, the potential influence of stabilised Criegee intermediates (sCI) on the reaction system was examined by addition of (1.0–1.5) × 10^{14} cm^{-3} SO_2 (Air Liquide, 99.9%) in one kinetic and two product study experiments. The rate coefficient was determined by the relative-rate method using E2-butene (Messer, 99%) and cyclohexene (Sigma-Aldrich, 99%) as reference compounds. Initial concentrations of 2,5-dimethylfuran (Sigma-Aldrich, 99%) were in the range (1.2–9.6) × 10^{13} cm^{-3}.

Instrumentation

The reaction mixtures were monitored using long-path FTIR spectroscopy and mass spectrometry. The FTIR spectrometer (Nicolet iS 50; Thermo Fisher Scientific) is operated with a liquid nitrogen cooled HgCdTe detector. The whole transfer optics housing, usually operated with dry air flushing, was purged with ultrapure nitrogen evaporated from a liquid nitrogen tank to allow monitoring of CO_2. The reliability of the CO_2 quantification was successfully proven in preceding work.[19,20] FTIR spectra were recorded in the spectral range of 4000–700 cm^{-1} at a resolution of 1 cm^{-1}. The time resolution of the FTIR data was varied in between the experiments by varying the number of scans co-added per spectrum between 20 and 50 resulting in averaging periods of about 32–81 s.

A PTR-Tof 8000 (Ionicon Analytik GmbH, Innsbruck, Austria) was connected on-line to the reaction chamber and operated in H_3O^+ mode. The drift tube of the PTR-Tof-MS was kept at a temperature of 70 °C, 2.3 mbar pressure and 510 V drift voltage, which resulted in a reduced electric field strength of $E/N \approx 120$ Td (1 Td = 1 × 10^{-17} V cm^2). The sampling line of the instrument was operated at a temperature of 70 °C and coupled to a heated stainless steel line mounted on the end flange of the 1080 L chamber. The sample flow was about 200 mL min^{-1}. Due to a lack of reliable calibration, the PTR-Tof-MS was used only for observing qualitatively the time profiles of the identified mass signals which were normalized by the m/z 21 ($H_3{}^{18}O^+$) signal.

Data analysis

The different substances were quantified *via* FTIR by manual subtraction with calibrated reference spectra from the internal laboratory database. For 2,5-dimethylfuran, acetic acid and acetic anhydride we used cross sections (base 10) of 3.8 × 10^{-18} cm $molecule^{-1}$ (1060–880 cm^{-1}), 2.6 × 10^{-19} cm^2

Open Access Article. Published on 19 8 2024. Downloaded on 2026/02/16 5:19:08.
This article is licensed under a Creative Commons Attribution 3.0 Unported Licence.

molecule^{-1} (1177 cm^{-1}), and 3.6 × 10^{-19} cm^2 molecule^{-1} (1778 cm^{-1}), respectively, which were determined in this study by injection of different known volumes into the chamber and applying the Beer–Lambert law. For ketene ($CH_2{=}C{=}O$), we used a cross section of 7.7 × 10^{-19} cm^2 molecule^{-1} (base 10) for the P-branch maximum at 2137 cm^{-1}. The derivation of this value is outlined in Section D of the ESI.† The plots used for the calculation of the cross sections as well as a list of all literature values used for the quantification are given in the ESI.† Overall quantification errors in the experiments consist mainly of the uncertainty assigned to the absorption cross section and the subtraction procedure. The latter error was estimated for each compound by checking the reproducibility of the subtraction in selected spectra. Consequently, estimated relative uncertainties are about 11% for acetic acid, 7% for acetic anhydride, 6% for 2,5-dimethylfuran, 6% for formaldehyde, 11% for glyoxal, 21% for ketene, 3% for methyl glyoxal, and 12% for methyl hydroperoxide, respectively.

The rate coefficient of the target reaction was determined using the relative-rate method which is based on relating the consumption of the target species to the consumption of a reference compound (ref) whose rate coefficient is accurately known. In the absence of significant wall losses, the rate coefficient can be determined by the following expression:

$$\ln\left(\frac{[25\mathrm{DMF}]_0}{[25\mathrm{DMF}]_t}\right) = \frac{k_{25\mathrm{DMF}}}{k_{\mathrm{ref}}} \times \ln\left(\frac{[\mathrm{ref}]_0}{[\mathrm{ref}]_t}\right) \quad (1)$$

Since the relative-rate method has been described extensively in the literature,[21] no further details on the derivation of the above equation will be given here. The recommended rate coefficients of 2.0 × 10^{-16} cm^3 molecule^{-1} s^{-1} (E2-butene)[22] and 7.8 × 10^{-17} cm^3 molecule^{-1} s^{-1} (cyclohexene)[23] were used for the calculation of $k_{25\mathrm{DMF}}$. The accuracy errors of these values are $\Delta\log k = 0.1$ for E2-butene[22] and about 14% for cyclohexene.[23]

Product yields were calculated by relating the formation of the product to the consumption of the target species (Δ25DMF). The values reported within this work result from regression analysis over the linear range of each yield plot. In order to identify causes of non-linear behaviour, the time profiles were also simulated using a modelling approach introduced in preceding work.[19] The profile of the initial reactant (25DMF), which is lost solely by reaction with O_3, is approximated until the modelled time profile matches the experimental data. Both the yield (constant over the entire experimental run) and the wall loss of a reaction product are introduced as a variable parameter to be adjusted until a reasonable match between experimental and modelled profile is achieved if possible. A more detailed description of the procedure is outlined in Section F of the ESI.†

Results and discussion

A total of 21 experiments was performed investigating the rate coefficient (EXP1–EXP3, EXP21), the OH production (EXP4–EXP11) and the product formation (EXP12–EXP20) of the 2,5-dimethylfuran + O_3 system. 25DMF did not exhibit a measurable wall loss in these experiments. The overall consumption of 25DMF was varied in the experiments and ranged from about 43% to 86%.

Rate coefficient

The use of two reference compounds and the resulting product formation during the reaction cause significant overlapping of absorption bands in the FTIR spectra, which hinders the spectral subtraction procedure. As a consequence, reliable subtraction was not possible in the case of cyclohexene and we only used the PTR-MS data for this compound. The relative-rate plots using the PTR-MS data are shown in Fig. 1. The rate coefficients obtained from these data agree within 13% (2σ).

The experimentally observed rate coefficient ratio of cyclohexene and E2-butene using the PTR data matches the value based on the currently recommended rate coefficients. This suggests the amount of scavenger was high enough to suppress any influence of OH.

Ozone generators based on electrical discharge might produce also nitrogen oxides and eventually reactive species like NO_3 radicals if trace amounts of N_2 are present in the high purity grade oxygen used to generate ozone. While this is typically not relevant for most VOCs, it might, in principle, interfere

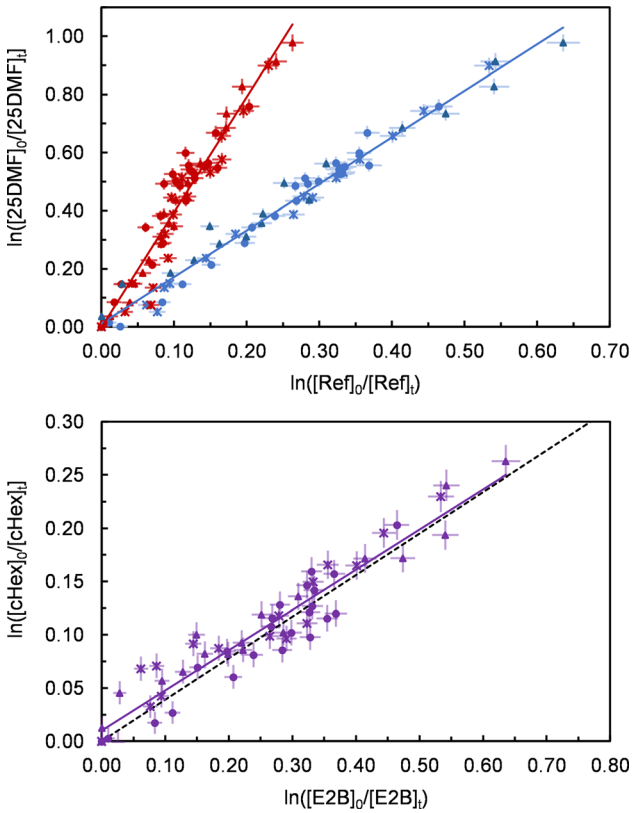

Fig. 1 Relative-rate plots of the 2,5-dimethylfuran + O_3 system using cyclohexene (red) and E2-butene (blue) as references (upper panel) and the crosscheck of both references (lower panel) using the PTR-MS data. The dotted line represents the theoretically expected rate coefficient ratio. Different experimental runs are denoted with different symbols. Error bars represent the 2σ statistical uncertainty.

 © 2024 The Author(s). Published by the Royal Society of Chemistry

Open Access Article. Published on 19 8 2024. Downloaded on 2026/02/16 5:19:08.
This article is licensed under a Creative Commons Attribution 3.0 Unported Licence.

in the present reaction system since 2,5-dimethylfuran is extremely reactive towards NO_3.[8] Yet, this interference were the largest during ozone addition and would slow down after the injection stops. As a consequence, significant non-linearity should be observed in the relative-rate plots, which is obviously not the case (Fig. 1). To ultimately rule out any influence of NO_3 an excess of ozone was added to 1 atm of synthetic air, in the absence of reactive VOCs, and monitored for about 1 hour in the dark. After that, 2,5-dimethylfuran was added at atmospheric pressure and the mixture stirred for about 3 min for homogenization. After this period, 25DMF was almost entirely consumed without any hint for the formation of organic nitrate species.

The rate coefficient obtained from the experiment with SO_2 added (EXP21) is indistinguishable from the values of experiments without SO_2 injection (EXP1–EXP3). Consequently, any reaction between 2,5-dimethylfuran and stabilised Criegee intermediates appears not relevant in the experiments. Overall, these findings give confidence that the loss of 2,5-dimethylfuran after O_3 addition is due to reaction with O_3 solely.

The final rate coefficient of $(3.3 \pm 1.0) \times 10^{-16}$ cm^3 molecule^{-1} s^{-1} was obtained from the weighted average of all individual determinations. The quoted errors represent an expanded, conservative accuracy error of 30% (2σ) to cover all potential uncertainties.

The present value is slightly smaller than the sole experimentally determined rate coefficient of $(4.2 \pm 0.9) \times 10^{-16}$ cm^3 molecule^{-1} s^{-1} reported by Matsumoto,[15] who followed the decay of ozone with a chemiluminescence detector for different initial 25DMF concentrations at 295 K. These values are roughly a factor of 2 smaller than suggested from theoretical calculations,[16] which is still in reasonable agreement considering the fact that the theoretical study overestimates the experimentally determined rate coefficient for furan[14] by a factor of ten.

OH production

The formation of OH radicals was investigated in separate experiments using 1,3,5-trimethylbenzene (135TMB) as an OH tracer. In order to check for potential influence of the experimental conditions on the OH yield calculation, we varied the initial reactant concentration ratio (25DMF/135TMB) in the experiments. Two subsets of experiments were performed in which either FTIR (EXP4–EXP6, ESI Table S1†) or PTR-MS (EXP7–EXP11, ESI Table S1†) was used to observe the time profiles of the target species and the OH tracer. In the latter, the FTIR was used solely to determine the initial reactant concentrations.

135TMB exhibits in these experiments a wall loss of up to 5×10^{-5} s^{-1}. Yet, the decay observed for 135TMB is definitely larger when O_3 is added to the mixture indicating the formation of OH in the reaction system. Plots of $\ln([135TMB]_0/[135TMB]_t)$ *vs.* time from data collected after one single O_3 injection appear linear within statistical errors, which suggests a near steady-state OH level in each experiment. OH concentrations estimated from these plots were in the range from (2–6) $\times 10^6$ cm^{-3}, respectively.

In the initial phase of the reaction, production and loss rate of OH are dominated by 25DMF and 135TMB:

$$25DMF + O_3 \rightarrow \alpha OH + \text{products} \quad (R1)$$

$$25DMF + OH \rightarrow \text{products} \quad (R2)$$

$$135TMB + OH \rightarrow \text{products} \quad (R3)$$

Accordingly, by extrapolating to the start of the reaction, the OH yield α can be calculated as follows:

$$\alpha = \frac{[OH](k_2[25DMF] + k_3[135TMB])}{k_1[25DMF][O_3]} \quad (2)$$

The detailed derivation of eqn (2) can be found in Section C of the ESI.†

As evident from Fig. 2, both the 25DMF/135TMB ratio and the analysis method did not influence the OH yield determination within the statistical uncertainties (2σ) but in two cases exceptionally high α-values were registered. Since consistently low OH yields were in most cases obtained from experiments performed after the chamber was conditioned with ozone, the most likely explanation is the OH yield determination was easily affected by OH production from the wall:

$$O_3 + \text{wall} \rightarrow \beta OH \quad (R4)$$

Combining the results of these experiments leads to an OH yield of 0.25 ± 0.06, depicted by the red range in Fig. 2. The error represents the statistical uncertainty (2σ). Yet, the overall accuracy error is certainly on the order of 40% when considering all uncertainties in the calculations. In addition, although the additional formation of OH, likely from the chamber wall, was largely minimized in these experiments, the OH yield should still be regarded as an upper limit since the reaction

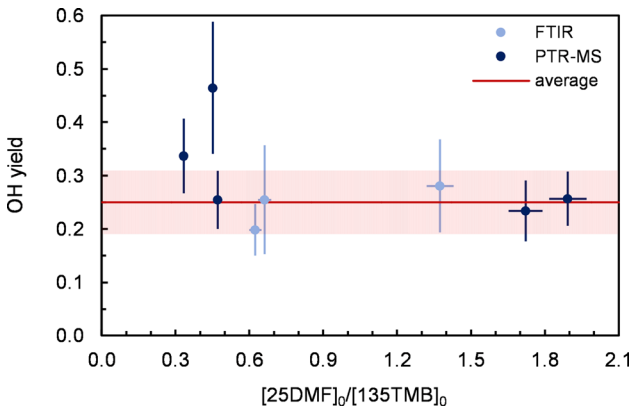

Fig. 2 OH yields determined under various ratios of the initial concentrations of the target compound (2,5-dimethylfuran) and the OH tracer (1,3,5-trimethylbenzene) using either FTIR (light blue) or PTR-MS (dark blue). Error bars represent the respective statistical uncertainty (2σ). The red line represents the average and the light red range shows the statistical uncertainty.

Open Access Article. Published on 19 8 2024. Downloaded on 2026/02/16 5:19:08.
This article is licensed under a Creative Commons Attribution 3.0 Unported Licence.

system itself might act as a secondary source of OH, *e.g.* through peroxy radical reactions:

$$RO_2 + HO_2 \rightarrow \gamma OH + \gamma RO + O_2 \quad (R5)$$

All this suggests that direct OH formation from the 2,5-dimethylfuran + O_3 reaction is rather low.

Product determination

Fig. 3 shows, exemplary, time profiles and product formation (for species quantified by FTIR) for one experiment. The experimental data are adequately reproduced by the simulated time profiles when assuming a constant product yield and a unimolecular loss. The levels of glyoxal and methyl hydroperoxide, in particular, decrease once the reaction rate slows down significantly. Yet, this behaviour was reproducible for most of the experiments. The time profiles of methyl hydroperoxide, for example, were reproduced for the entire experimental duration when considering k_{wall} in the range of $(0.5–1.7) \times 10^{-3}$ s^{-1} in the model calculation. Such large values can be explained by the constant stirring inside the chamber which might accelerate the loss rate for species exhibiting wall affinity, which is likely the case for methyl hydroperoxide (CH_3OOH). Only in EXP19 and EXP20, which were performed at a later stage, the CH_3OOH wall loss was almost zero.

For methyl glyoxal, the model runs tend to either overestimate the experimental data in the beginning or underestimate the data in the end of the experiment like it is the case in

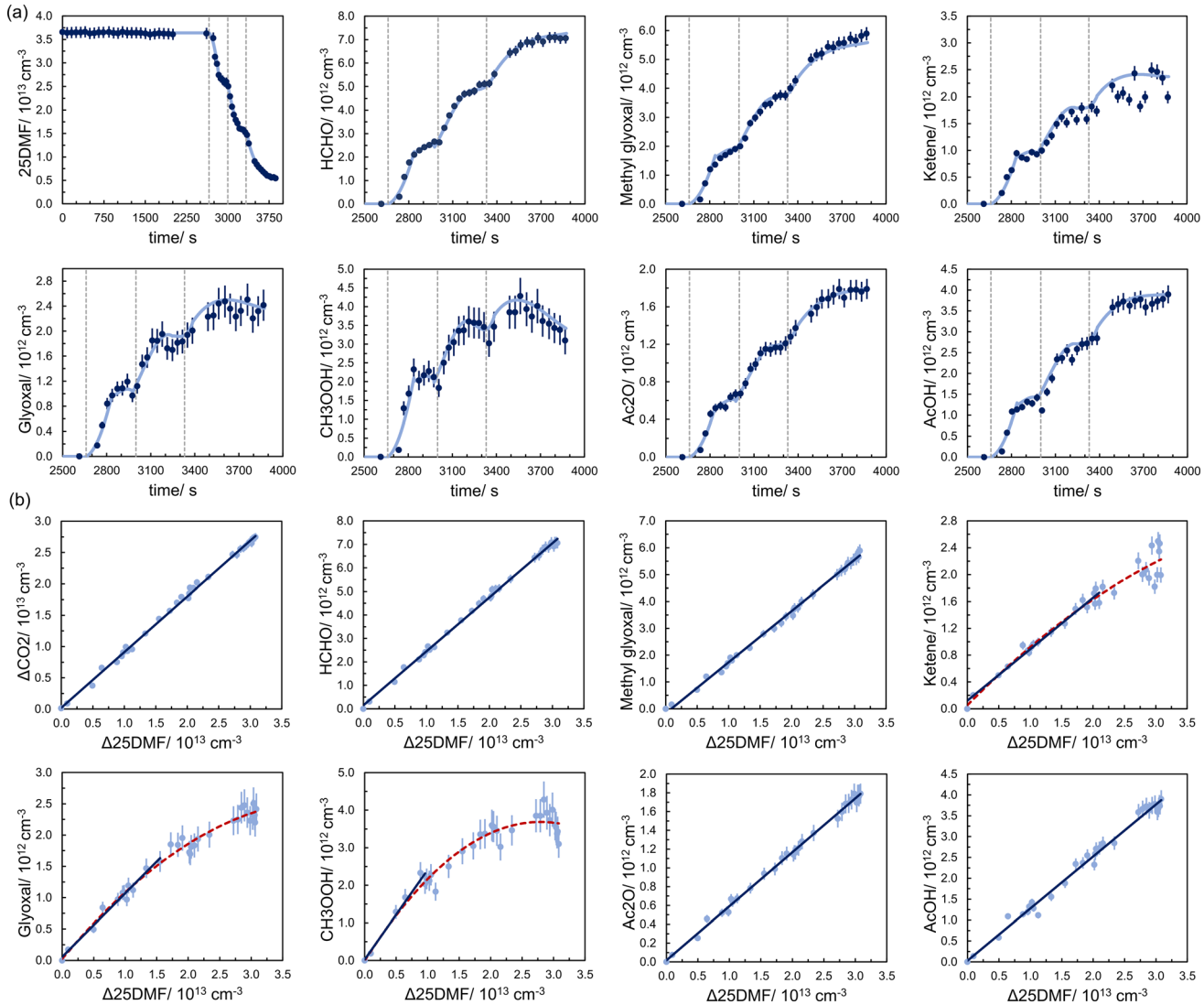

Fig. 3 (a) Concentration–time profiles of quantified species in EXP13. Dark blue dots represent measured data (FTIR) together with the respective statistical uncertainty (2σ). The light blue lines represent the modelled time profiles (best-fit) considering a constant formation yield and a first-order wall loss. The vertical dotted lines mark the respective start of O_3 addition for a period of about 1 min. (b) Yield plots of quantified species in EXP13. Light blue dots represent measured data (FTIR) together with the respective statistical uncertainty (2σ). The solid blue lines represent the linear fit obtained through regression analysis. The dotted red lines represent polynomial functions to aid visual inspection of the non-linearity.

 © 2024 The Author(s). Published by the Royal Society of Chemistry

Open Access Article. Published on 19 8 2024. Downloaded on 2026/02/16 5:19:08.
This article is licensed under a Creative Commons Attribution 3.0 Unported Licence.

EXP13 (Fig. 3). In the yield plots this is reflected in a minute curvature which might indicate a larger methyl glyoxal yield at higher 25DMF consumption levels. Yet, the deviation from linearity is extremely close to the precision error and cannot be confirmed unambiguously.

Overall, the time profiles and yield plots suggest the formation of these species as first-generation products. The yields, obtained through regression analysis over the linear range of the plots, are in the range 23.0–24.4% for formaldehyde (HCHO), 15.1–20.0% for methyl glyoxal, 8–10% for ketene, 7–12% for glyoxal, 18–31% for CH_3OOH, 4.8–6.2% for acetic anhydride, and 10–13% for acetic acid, respectively. Yield plots and time profiles of all product study experiments can be found in Section E of the ESI.†

The CO_2 yields exhibit significant scatter and range from 81% to 107%. Since CO was used as an OH scavenger, production of CO_2 arises from CO + OH. Consequently, the variation in the observed CO_2 yield appears at least in part consistent with the observations from the OH tracer experiments. Yet, since the lower limit of the CO_2 yield appears reproducible and is still more than a factor of 3 larger than the upper limit determined for the OH yield, a significant fraction of CO_2 originates likely from 2,5-dimethylfuran + O_3 itself.

The FTIR residual spectra (see Fig. S30 of the ESI†) do indicate additional unidentified reaction products. The absorption pattern in the range 1840–1600 cm^{-1} suggests the presence of different carbonyl groups. In addition, the absorption band centred at 1645 cm^{-1} might suggest the presence of unsaturated reaction products containing a C=C bond. The most prominent absorption bands are centred at 1203 cm^{-1} and 1161 cm^{-1}, which strongly suggest the formation of species containing C–O bonds. Absorption bands centred at 3586 cm^{-1} and 3499 cm^{-1} could correspond to a combination of O–H stretching vibrations and an overtone of C–O stretching vibrations.

Table 1 Signals (*m*/*z*) observed in all product study experiments monitored with the PTR-MS instrument

m/*z*	Formula	Assignment
31.02	CH_3O^+	Formaldehyde, glyoxal fragment
41.04	$C_3H_5^+$	*Propyne* + fragments[a]
43.02	$C_2H_3O^+$	Ketene + fragments
45.03	$C_2H_5O^+$	Methyl glyoxal fragment
59.01	$C_2H_3O_2^+$	Glyoxal
59.05	$C_3H_7O^+$	n.a.
61.03	$C_2H_5O_2^+$	Acetic acid, acetic anhydride
73.03	$C_3H_5O_2^+$	Methyl glyoxal, *tricarbonyl (9) fragment*[a]
75.04	$C_3H_7O_2^+$	*Hydroxydicarbonyl (10) fragment*[a]
85.03	$C_4H_5O_2^+$	n.a.
87.04	$C_4H_7O_2^+$	n.a.
103.04	$C_4H_7O_3^+$	*Hydroxydicarbonyl (10)*[a]
113.06	$C_6H_9O_2^+$	*Epoxide*[a]
117.05	$C_5H_9O_3^+$	n.a.
145.05	$C_6H_9O_4^+$	n.a.

[a] Assignment of species in italics remains uncertain and is tentative only, n.a. = not assigned, numbers in parentheses correspond to the numbering used in the mechanistic schemes.

Table 1 summarizes mass signals whose build-up was observed during the reaction. The assignment remains, however, incomplete and in the majority of cases the *m*/*z* signals are not unique for a single species formed in the reaction system. For example, both HCHO and glyoxal contribute to *m*/*z* 31 (CH_3O^+) whereas fragments of methyl glyoxal (*m*/*z* 73, $C_3H_5O_2^+$) contribute to *m*/*z* 45. A fragment of a tricarbonyl likely contributes also to *m*/*z* 73. Tentative assignments, where possible, are discussed below in conjunction with a possible ozonolysis mechanism. The temporal evolution of the mass signals is provided in Section H of the ESI.†

Mechanism

The reaction products suggest the initial step of the 25DMF + O_3 reaction proceeds dominantly through the concerted 1,3-cycloaddition resulting in a primary ozonide (POZ, Scheme 1). The *m*/*z* 113 signal ($C_6H_9O_2^+$) could technically correspond to a protonated epoxide. In contrast to simple alkenes epoxide formation accounts indeed for up to 5% of the reaction of acyclic conjugated dienes such as isoprene with O_3.[24] However, the assignment of *m*/*z* 113 remains uncertain and there is no clear evidence for epoxide formation in the FTIR spectra. Accordingly, we can neither rule out nor prove the existence of an epoxide pathway.

The exothermicity of the 1,3-cycloaddition causes a prompt decomposition of the vibrationally excited POZ. Since there is no hint for products arising from a stepwise POZ dissociation route (O'Neil–Blumstein mechanism[25]), the POZ decomposition will likely proceed through two pathways and yield Criegee intermediates (CI) with a yield of unity. In both cases the carbonyl and the carbonyl oxide ($C{=}O^+{-}O^-$) group remain within the same molecule, either adjacent to the remaining C=C bond and the former heterocyclic O atom (hereafter

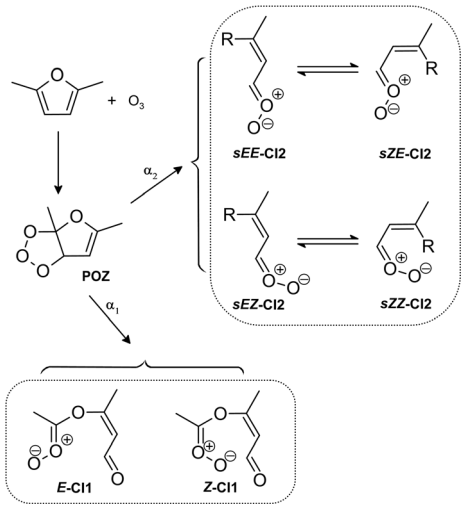

Scheme 1 Initial steps of the ozonolysis of 2,5-dimethylfuran and the (carbonyl oxides = Criegee Intermediates, CI) formed following decomposition of the primary ozonide (POZ). The *E*/*Z*-nomenclature follows the Cahn–Ingold–Prelog priority rules. For clarity and in the absence of ESI,† no differentiation between chemically activated and stabilized CI is drawn. R = $-OC(=O)CH_3$ for readability reasons.

Open Access Article. Published on 19 8 2024. Downloaded on 2026/02/16 5:19:08.
This article is licensed under a Creative Commons Attribution 3.0 Unported Licence.

referred to as CI1) or *vice versa* (hereafter referred to as CI2), respectively (Scheme 1). Minimum two stereoisomers are possible for both Criegee Intermediates (CI) due to the orientation of the outer O atom of the carbonyl oxide (Scheme 1). The *E*/*Z*-nomenclature used here follows the Cahn–Ingold–Prelog priority rules.

The carbonyl oxide group is part of a conjugated π-system in CI2. For these type of carbonyl oxides, theoretical calculations suggest internal rotation along the central single bond to be fast enough to reach an equilibrium between the conformers when the CI are stabilised.[26] As a consequence, they are assumed to act as a single species.

The loss of SO_2 in EXP 19 and EXP 20 is <2% and corresponds to a $\Delta SO_2/\Delta 25DMF$ of <4%. Moreover, the product distribution was not measurably affected by the addition of SO_2 suggesting that either the fraction of CI which is stabilised is very low or unimolecular reactions dominate over bimolecular processes even for the sCI. For simplicity and in the absence of additional information, we will not further differentiate between excited and stabilised CI in the following discussion.

The *m*/*z* 145 signal ($C_6H_9O_4^+$) suggests the formation of species retaining the carbon skeleton. In principle, the dioxirane route is accessible for most of the CI. Further isomerization will yield initially vibrationally excited acids and/or esters, which easily decompose. Yet, as observed for CI originating from some terpene ozonolysis,[27,28] it appears possible that excited acids (or esters) from larger CI – like those cast from 25DMF + O_3 – are stabilized by collision. Each of these species would contain two carbonyl groups with different chemical environments. Generally, this would be in accordance with the remaining carbonyl absorptions observed in the FTIR residual spectra.

The presence of both functionalities in the intermediate enables also an intramolecular reaction of the carbonyl oxide with the carbonyl group, in principle. If the internal energy distribution allows stabilisation, this might finally result in the formation of stabilised secondary ozonides (SOZ), which might contribute to the intense C–O absorption bands present in the FTIR residual spectra. The *m*/*z* 145 signal would correspond to protonated SOZ. Yet, it remains unclear if the SOZ structure remains intact after a proton transfer reaction.

Overall, the experimental clues towards formation of products retaining the C_6 core structure are rather surprising. SOZ as well as acid formation (following the dioxirane route) was observed previously particularly for sesquiterpenes (C_{15}).[27,28] It appears that the excitation level of the present CI is rather low although all quantified reaction products confirm that CI fragmentation is still significant. Pathways accounting for those products are subsequently discussed below.

***Z*-CI1.** The orientation of the outer O atom in *Z*-CI1 precludes an 1,4-H shift isomerisation, causing the most likely pathway to be isomerisation into a dioxirane intermediate (Scheme 2). Subsequent ring-opening yields the corresponding bis(oxy) biradical, which is lost by either decomposition or further isomerisation into a vibronically excited carbonate. Theoretical calculations[28,29] suggest decomposition to be the dominant pathway for bis(oxy) biradicals formed from stabilised CI (after

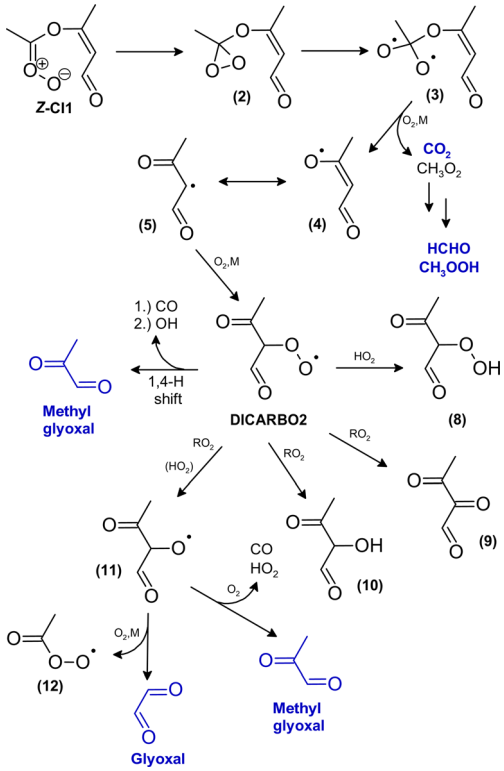

Scheme 2 Proposed mechanism for the fate of the carbonyl oxide *Z*-CI1 yielding in fragmentation of the C_6 core structure. Species which were clearly identified as reaction products are marked in blue.

intersystem crossing). Accordingly, fragmentation of *Z*-CI1 yields CO_2, CH_3 radicals and a vinoxy-type radical (4, Scheme 2). The bimolecular reactions of the consecutively formed CH_3O_2 radical account for the formation of formaldehyde and methyl hydroperoxide as observed in the reaction system.

Vinoxy-type radicals are typically considered as in equilibrium with the corresponding alkyl radical. Consequently, the most likely pathway is addition of oxygen yielding finally a thermalized carbonyl-substituted peroxy radical (DICARBO2, Scheme 2) at atmospheric pressure. Since the background level of NO is virtually zero after O_3 addition, conventional bimolecular reactions of DICARBO2 are supposedly dominated by reaction with RO_2 or HO_2, respectively. Possible directly formed closed-shell reaction products are a multifunctional hydroperoxide (*via* DICARBO2 + HO_2), a hydroxydicarbonyl and/or a tricarbonyl species (both through RO_2 permutation reactions). In principle, these species might be present in the FTIR residual spectra as indicated by the presence of several different carbonyl absorption features. The PTR-MS data likely support the formation of the hydroxydicarbonyl (*m*/*z* 103, 75) and the tricarbonyl (*m*/*z* 73) compound.

For the alkoxy radical, formed from DICARBO2 by RO_2 permutation reactions and possibly by HO_2, decomposition is likely to be thermodynamically favoured due to the substitution pattern on both α-C atoms. The fragmentation yields either glyoxal + CHO or methyl glyoxal + an acetyl radical ($CH_3C(O)$). Accordingly, the alkoxy radical of DICARBO2 provides one

 © 2024 The Author(s). Published by the Royal Society of Chemistry

Open Access Article. Published on 19 8 2024. Downloaded on 2026/02/16 5:19:08.
This article is licensed under a Creative Commons Attribution 3.0 Unported Licence.

possible explanation for the formation of both dicarbonyls. The co-product of methyl glyoxal is immediately converted into an acetyl peroxy radical. Under the experimental conditions, the further chemistry would evolve into CH_3O_2 radicals (and the subsequent closed-shell reaction products), CO_2, acetic acid and peracetic acid (PAA). However, the acetic acid yield is significantly larger than possible when considering only the acetyl peroxy radical reaction scheme (see *e.g.* Jenkin *et al.*[30] and references therein) and strongly suggests another predominant source in the reaction system. In addition, there is no clear evidence for the formation of peracetic acid; we derive an upper limit of only 2% for the PAA yield based on the residual FTIR spectra.

DICARBO2 exhibits an aldehydic H atom close to the peroxy group which facilitates H-shift isomerisation reactions. These reactions are typically considered only at low radical concentrations close to atmospheric conditions since at higher peroxy radical levels bimolecular reactions predominate. However, both combined experimental and theoretical work on the methacrolein oxidation[31] as well as SAR predictions[32] indicate that H-shift isomerisation reactions are extremely rapid for peroxy radicals containing an aldehyde group. This pathway would provide an additional (small) source of OH and account for the formation of methyl glyoxal without producing acetyl (peroxy) radicals.

The fraction of DICARBO2 undergoing unimolecular isomerisation would be sensitive to the overall RO_2^* level, where RO_2^* denotes the sum of individual RO_2 species and HO_2.

$$RO_2^* = \sum_i RO_2{}^i + HO_2 \tag{3}$$

Although the exact concentration of RO_2^* is not known, the steady-state level is expected to be roughly proportional to the production rate of peroxy radicals ($P_{RO_2^*}$). As such, the loss rate of 2,5-dimethylfuran can be used as a proxy for the overall peroxy radical level in the system:

$$P_{RO_2^*} = \phi \times k_1[25DMF][O_3] \tag{4}$$

Here, φ denotes an unknown, dimensionless factor representing the overall RO_2^* yield.

In order to assess whether product yields are sensitive to the RO_2^* level in the system we tried to vary $P_{RO_2^*}$ by changing both the initial concentration of 25DMF and the 25DMF loss rate in the different product study experiments. For each experiment, we determined an average $P_{RO_2^*}$ by considering only the time intervals, where significant consumption of 2,5-dimethylfuran is observed. The product yields in dependence of $P_{RO_2^*}$ are shown in Fig. 4. It appears that a dependence is observed only for HCHO, glyoxal and methyl glyoxal. Both the HCHO and glyoxal yield increase with rising $P_{RO_2^*}$, whereas the methyl glyoxal yield decreases. In addition, the effect is much more pronounced in the case of methyl glyoxal, yielding a relative decrease of about 23% within the experimental limits compared to a relative increase of about 4% for HCHO.

The increasing methyl glyoxal yield associated with a lower overall peroxy radical level supports the above hypothesis of a unimolecular pathway forming methyl glyoxal. Accordingly, the 1,4-H shift isomerisation of DICARBO2 appears competitive to bimolecular processes under the experimental conditions. The SAR approach[32] yields k_{uni} of about 7×10^{-2} s^{-1}. Considering RO_2 and HO_2 levels inferred from previous work under similar experimental conditions[33] a bimolecular loss rate in the order of 10^{-1} s^{-1} can be estimated when assuming average rate coefficients of 10^{-11} cm^3 $molecule^{-1}$ s^{-1} for the bimolecular processes, which is consistent with both the experimental observations as well as the SAR estimate. The opposite trend in the product yields, particularly for glyoxal, is consistent with the bimolecular loss of DICARBO2 and the decomposition of the subsequently formed alkoxy radical (11, Scheme 2).

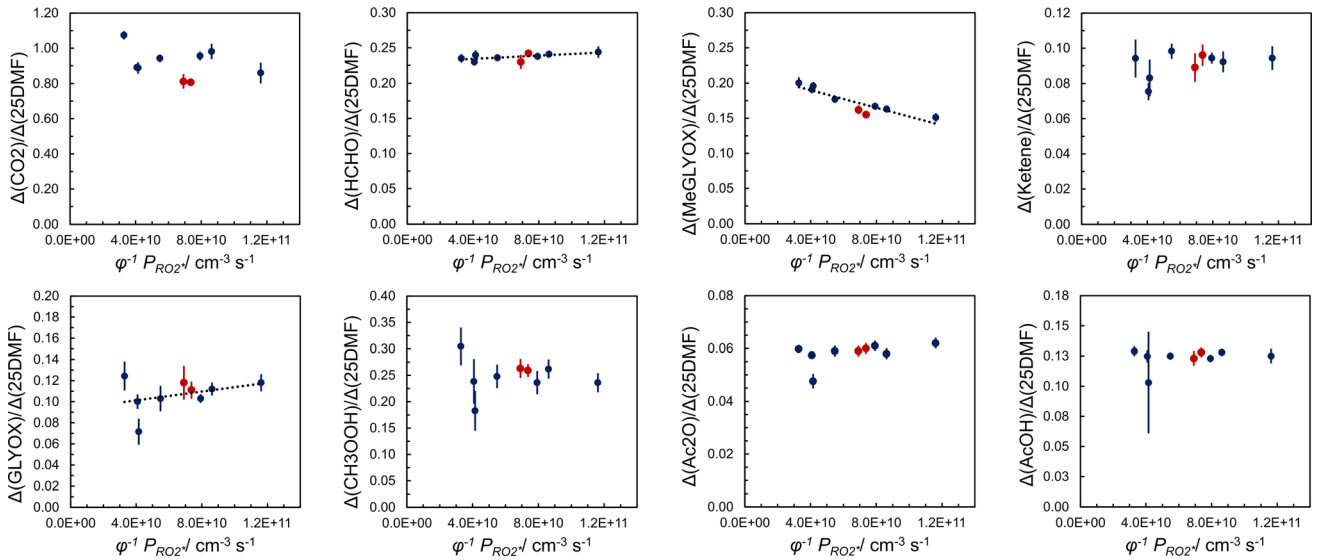

Fig. 4 Variation of product yields with $P_{RO_2^*}$. Error bars represent 2σ statistical uncertainties resulting from regression analysis. The yields obtained from the experiments with SO_2 added are marked in red.

Open Access Article. Published on 19 8 2024. Downloaded on 2026/02/16 5:19:08.
This article is licensed under a Creative Commons Attribution 3.0 Unported Licence.

The rovibronically excited carbonate (omitted for legibility reasons in Scheme 2) might theoretically be stabilised by collision and contribute to the *m*/*z* 145 signal. Though, fragmentation, particularly the release of CO_2, appears likely. Scission may occur at different bonds in the carbonate molecule, in order that several fragmentation pathways appear possible, in general. Decomposition would yield, at least partly, the same species as fragmentation of the bis(oxy) biradical.

***E*-CI1.** *E*-CI1 is the only carbonyl oxide formed in the reaction system for which 1,4-H shift isomerisation is accessible and likely to be the predominant loss pathway (Scheme 3). If none of the possible CI is preferred, *E*-CI1 will account for about 25% of the carbonyl oxides formed in the reaction system, which appears highly consistent with the OH yield estimate presented above.

As discussed for DICARBO2, bimolecular reactions of the subsequently formed peroxy radical (19, Scheme 3) will be dominated by reaction with RO_2 and HO_2. However, the experimental data do not clearly support the consecutive formation of a multifunctional hydroperoxide, a hydroxydicarbonyl and/or tricarbonyl species. The corresponding alkoxy radical will likely decompose and contribute to the formation of HCHO and CO_2.

The further fate of the remaining vinyl-type radical (24, Scheme 3) remains rather speculative. Such radicals are known from combustion chemistry and reactions with O_2 were investigated particularly for low pressure conditions. Investigations, *e.g.* for the reaction of the vinyl radical with O_2, suggest a mechanism involving a 3- or 4-membered transition state yielding predominantly HCHO + CHO or HCHO + H + CO, respectively.[34–36] A detailed product analysis study on the C_2H_3 + O_2 reaction combined with theoretical calculations suggest the mechanism to be valid even at room temperature and atmospheric pressure with the majority of CHO radicals promptly dissociating.[37] Based on that, the most probable pathway is the reaction with O_2 yielding glyoxal + $CH_3C(O)$ and/or glyoxal + CH_3 + CO, respectively.

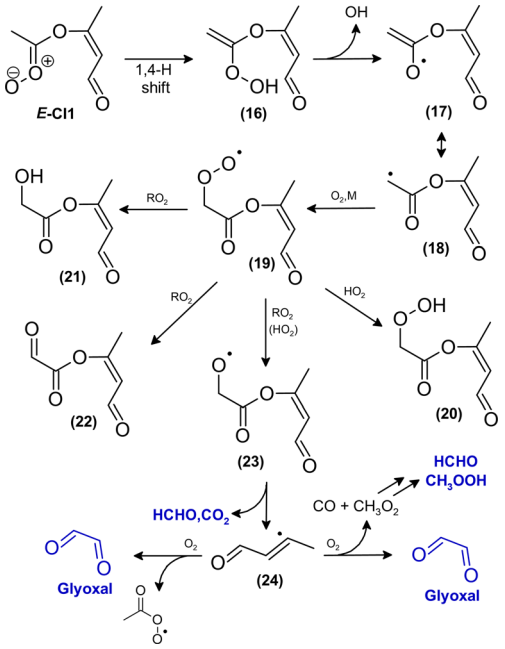

Scheme 3 Proposed mechanism for the fate of the carbonyl oxide *E*-CI1 following 1,4-H isomerisation. Species which were clearly identified as reaction products are marked in blue.

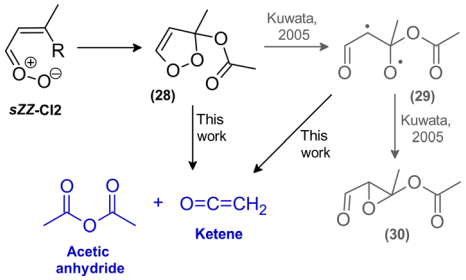

Scheme 4 Proposed mechanism for the fate of the carbonyl oxide s*ZZ*-CI2 following 1,5-ring closure. Species which were clearly identified as reaction products are marked in blue. R = −OC(=O)CH_3 for readability reasons.

s*EZ*-CI2/s*ZZ*-CI2. For the s*Z*-conformer of *Z*-CI2 there exists the possibility of a 1,5-ring closure yielding a dioxolene intermediate (28, Scheme 4). This pathway was originally proposed by Kuwata *et al.*[38] for methyl vinyl ketone oxide formed in the isoprene ozonolysis. The theoretical study did further suggest this channel to be favoured over collisional stabilization, the dioxirane route as well as an 1,4-H shift isomerisation.[38] As a consequence, dioxolene formation appears to be likely the predominant loss pathway for *Z*-CI2.

Kuwata *et al.*[38] suggested the subsequent opening of the dioxolene intermediate resulting in a biradical (29, Scheme 4) that finally yields an epoxide species (30, Scheme 4). In fact, the formation of the epoxide remains unsettled, *e.g.* it might contribute to the *m*/*z* 145 signal ($C_6H_9O_4^+$). On the other hand, the FTIR residual spectra do not unambiguously show the presence of epoxides, as mentioned above.

Yet, in contrast to methyl vinyl ketone oxide, s*ZZ*-CI2 possesses an α-hydrogen atom which might be subject of migration, either in the biradical species or the dioxolene intermediate itself (Scheme 4). In both cases, the products are acetic anhydride and ketene, which are found in the reaction system. However, considering the respective accuracy errors, the average ketene/acetic anhydride ratio of about 1.6 likely suggests an additional source of ketene in the system.

s*EE*-CI2/s*ZE*-CI2. For *E*-CI2 the dioxirane route appears to be likely the predominant loss pathway, irrespective of the relative orientation of the C=C and C=O bond. The bis(oxy) biradical will either decompose or further isomerize into a functionalized acid with excess internal energy (36, Scheme 5). The fragmentation of the biradical would also contribute to the formation of CO_2. Yet, the further fate of the resulting unsaturated radical is rather unclear. The excited acid will either be stabilized by collision or fragment.

To date, there are only few studies on decomposition of vibrationally excited acids, mainly on formic and acetic acid (see *e.g.* Cox *et al.*[22] and Newland *et al.*[39] and references therein).

 © 2024 The Author(s). Published by the Royal Society of Chemistry

Open Access Article. Published on 19 8 2024. Downloaded on 2026/02/16 5:19:08.
This article is licensed under a Creative Commons Attribution 3.0 Unported Licence.

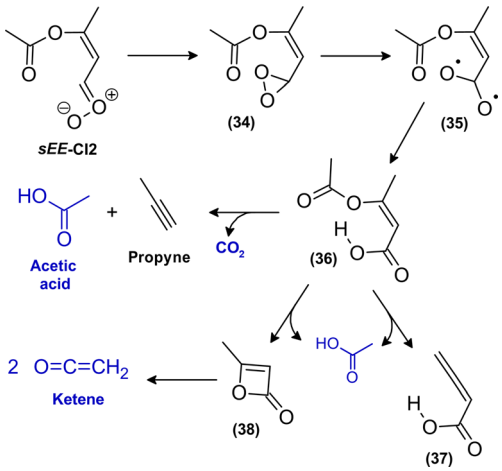

Scheme 5 Proposed mechanism for the fate of the carbonyl oxide s*EE*-CI2 following the dioxirane route. The same pathway is accessible for s*ZE*-CI2. Species which were clearly identified as reaction products are marked in blue.

Though, a common trait of chemically activated acids seems to be that fragmentation occurs *via* several pathways yielding either closed-shell molecules through rearrangement of chemical bonds or radical species initiated by bond scission. Recently, decarboxylation was also reported for excited trifluoroacetic acid resulting from a series of ozonolysis reactions.[40] In the present system, isopropenyl acetate would be the co-product of such a decarboxylation channel, for which we find no evidence in neither the FTIR residual spectra nor PTR-MS data.

Given the molecular structure, *E*-CI2 appears the likely source of the non-RO_2 acetic acid, which requires an H atom transfer in the chemically activated acid (36, Scheme 5), either from the OH or the CH_3 group. In the latter case, an allene (R–C=C=CH_2) is formed as a co-product (37, Scheme 5). The shift from the OH group might proceed *via* a 6-membered transition state yielding either the co-products propyne + CO_2 or an oxetene intermediate (38, Scheme 5), which might readily or even promptly rearrange to ketene.

The accessibility of these pathways needs certainly to be examined by theoretical calculations. Both, propyne and the allene-type compound are highly endothermic species. There is no experimental evidence for the existence of an allene although it could technically correspond to the *m*/*z* 85 ($C_4H_5O_2^+$) signal. In the propyne channel the co-product CO_2 acts as a strong thermodynamic sink. The formation of the alkyne might be argued by the presence of *m*/*z* 41 ($C_3H_5^+$) although this ion signal is typically considered to be a fragment, *e.g.* known from isoprene.[41] However, at present we do not find any other species in the proposed mechanism that could potentially yield $C_3H_5^+$ fragments. In the FTIR residual spectra, a small absorption with a peak centred at 3334 cm^{-1} might correspond to propyne. Yet, this assignment remains uncertain. Based on available absorption cross sections[42] the increase in this absorption feature would correspond to a yield of about 3% in the initial phase of the reaction.

The rearrangement of the oxetene intermediate (38, Scheme 5) is potentially the additional pathway necessary to explain the ketene yield observed, as discussed above. However, overall it seems that none of the proposed channels alone is able to account for the acetic acid yield suggesting a combination of these pathways and/or that additional unidentified reaction channels exist in the oxidation scheme.

Conclusions

The present work confirms that furan derivatives are reactive towards ozone. Particularly substituted furans like 2,5-dimethylfuran exhibit a reactivity towards O_3 similar to highly reactive monoterpenes like limonene or β-myrcene (see *e.g.* Cox *et al.*[22] and references therein). Other higher substituted furans will likely possess similar reactivity towards ozone. The main atmospheric sink remains the reaction with OH under most daytime conditions. Yet, it appears that O_3 chemistry of furan derivatives is not negligible, particularly under nighttime conditions. The ozonolysis of 2,5-dimethylfuran was shown to produce a range of small reactive (di)carbonyls, which are readily oxidized by OH and contribute to radical production by photolysis under typical daytime conditions. In addition, the reaction was shown to contribute to atmospheric acidity by forming acetic acid and acetic anhydride. This appears not substantially relevant for the atmosphere when considering a single compound. However, although the acetic acid pathways proposed here require confirmation, they are potentially valid for all furan derivatives possessing a CH_3 group in position 2. As such, these channels might contribute to organic acid formation inside nighttime BB plumes, which appears indeed underpredicted by current global models[43]

As said above, the present work intends to serve as a starting point for development of a comprehensive reaction scheme for the O_3 chemistry of furans. Yet, there is clearly a need for further research. The carbon balance is still below 50% and although we were able to identify a unimolecular pathway of RO_2, additional experiments should be performed under conditions closer to atmospheric radical levels. Further, there is certainly a need for theoretical calculations to assess the accessibility of reaction pathways proposed within this work.

Data availability

The data supporting this article have been included as part of the ESI.†

Conflicts of interest

There are no conflicts to declare.

Acknowledgements

NI gratefully acknowledges Iulia Patroescu-Klotz and Peter Wiesen for support and encouragement to develop own research ideas. The laboratory infrastructure used in this study is supported by the German Federal Ministry for Education and Research (BMBF) under grant agreement 01LK2001H (ACTRIS-D).

Open Access Article. Published on 19 8 2024. Downloaded on 2026/02/16 5:19:08.
This article is licensed under a Creative Commons Attribution 3.0 Unported Licence.

References

1 A. Jaswal, P. P. Singh and T. Mondal, Furfural – a versatile, biomass-derived platform chemical for the production of renewable chemicals, *Green Chem.*, 2022, **24**, 510–551.

2 Y. Román-Leshkov, C. J. Barrett, Z. Y. Liu and J. A. Dumesic, Production of dimethylfuran for liquid fuels from biomass-derived carbohydrates, *Nature*, 2007, **447**, 982–985.

3 M. Müller, B. E. Anderson, A. J. Beyersdorf, J. H. Crawford, G. S. Diskin, P. Eichler, A. Fried, F. N. Keutsch, T. Mikoviny, K. L. Thornhill, J. G. Walega, A. J. Weinheimer, M. Yang, R. J. Yokelson and A. Wisthaler, In situ measurements and modeling of reactive trace gases in a small biomass burning plume, *Atmos. Chem. Phys.*, 2016, **16**, 3813–3824.

4 L. E. Hatch, R. J. Yokelson, C. E. Stockwell, P. R. Veres, I. J. Simpson, D. R. Blake, J. J. Orlando and K. C. Barsanti, Multi-instrument comparison and compilation of non-methane organic gas emissions from biomass burning and implications for smoke-derived secondary organic aerosol precursors, *Atmos. Chem. Phys.*, 2017, **17**, 1471–1489.

5 A. Bierbach, I. Barnes and K. H. Becker, Rate coefficients for the gas-phase reactions of hydroxyl radicals with furan, 2-methylfuran, 2-ethylfuran and 2,5-dimethylfuran at 300 ± 2 K, *Atmos. Environ.*, 1992, **26**, 813–817.

6 A. Bierbach, I. Barnes and K. H. Becker, Product and kinetic study of the OH-initiated gas-phase oxidation of furan, 2-methylfuran and furanaldehydes at ≈300 K, *Atmos. Environ.*, 1995, **29**, 2651–2660.

7 C. A. Whelan, J. Eble, Z. S. Mir, M. A. Blitz, P. W. Seakins, M. Olzmann and D. Stone, Kinetics of the Reactions of Hydroxyl Radicals with Furan and Its Alkylated Derivatives 2-Methyl Furan and 2,5-Dimethyl Furan, *J. Phys. Chem. A*, 2020, **124**, 7416–7426.

8 M. J. Newland, Y. Ren, M. R. McGillen, L. Michelat, V. Daële and A. Mellouki, NO_3 chemistry of wildfire emissions: a kinetic study of the gas-phase reactions of furans with the NO_3 radical, *Atmos. Chem. Phys.*, 2022, **22**, 1761–1772.

9 M. M. Coggon, C. Y. Lim, A. R. Koss, K. Sekimoto, B. Yuan, J. B. Gilman, D. H. Hagan, V. Selimovic, K. J. Zarzana, S. S. Brown, J. M. Roberts, M. Müller, R. Yokelson, A. Wisthaler, J. E. Krechmer, J. L. Jimenez, C. Cappa, J. H. Kroll, J. de Gouw and C. Warneke, OH chemistry of non-methane organic gases (NMOGs) emitted from laboratory and ambient biomass burning smoke: evaluating the influence of furans and oxygenated aromatics on ozone and secondary NMOG formation, *Atmos. Chem. Phys.*, 2019, **19**, 14875–14899.

10 Z. C. J. Decker, K. J. Zarzana, M. Coggon, K.-E. Min, I. Pollack, T. B. Ryerson, J. Peischl, P. Edwards, W. P. Dubeì, M. Z. Markovic, J. M. Roberts, P. R. Veres, M. Graus, C. Warneke, J. de Gouw, L. E. Hatch, K. C. Barsanti and S. S. Brown, Nighttime Chemical Transformation in Biomass Burning Plumes: A Box Model Analysis Initialized with Aircraft Observations, *Environ. Sci. Technol.*, 2019, **53**, 2529–2538.

11 W. M. Jolly, M. A. Cochrane, P. H. Freeborn, Z. A. Holden, T. J. Brown, G. J. Williamson and D. M. J. S. Bowman, Climate-induced variations in global wildfire danger from 1979 to 2013, *Nat. Commun.*, 2015, **6**, 7537.

12 B. J. Harvey, Human-caused climate change is now a key driver of forest fire activity in the western United States, *Proc. Natl. Acad. Sci. U. S. A.*, 2016, **113**, 11649–11650.

13 R. J. Yokelson, J. D. Crounse, P. F. DeCarlo, T. Karl, S. Urbanski, E. Atlas, T. Campos, Y. Shinozuka, V. Kapustin, A. D. Clarke, A. Weinheimer, D. J. Knapp, D. D. Montzka, J. Holloway, P. Weibring, F. Flocke, W. Zheng, D. Toohey, P. O. Wennberg, C. Wiedinmyer, L. Mauldin, A. Fried, D. Richter, J. Walega, J. L. Jimenez, K. Adachi, P. R. Buseck, S. R. Hall and R. Shetter, Emissions from biomass burning in the Yucatan, *Atmos. Chem. Phys.*, 2009, **9**, 5785–5812.

14 R. Atkinson, S. M. Aschmann and W. P. L. Carter, Kinetics of the reactions of O_3 and OH radicals with furan and thiophene at 298 ± 2 K, *Int. J. Chem. Kinet.*, 1983, **15**, 1761–1772.

15 J. Matsumoto, Kinetics of the Reactions of Ozone with 2,5-Dimethylfuran and Its Atmospheric Implications, *Chem. Lett.*, 2011, **40**, 582–583.

16 M. Li, Y. Li and L. Wang, Gas-phase ozonolysis of furans, methylfurans, and dimethylfurans in the atmosphere, *Phys. Chem. Chem. Phys.*, 2018, **20**, 24735–24743.

17 M. Tajuelo, D. Rodríguez, A. Rodríguez, A. Escalona, G. Viteri, A. Aranda and Y. Diaz-de-Mera, Secondary organic aerosol formation from the ozonolysis and oh-photooxidation of 2,5-dimethylfuran, *Atmos. Environ.*, 2021, **245**, 118041.

18 A. Alvarado, R. Atkinson and J. Arey, Kinetics of the gas-phase reactions of NO_3 radicals and O_3 with 3-methylfuran and the OH radical yield from the O_3 reaction, *Int. J. Chem. Kinet.*, 1996, **28**, 905–909.

19 N. Illmann, R. G. Gibilisco, I. G. Bejan, I. Patroescu-Klotz and P. Wiesen, Atmospheric oxidation of α,β-unsaturated ketones: kinetics and mechanism of the OH radical reaction, *Atmos. Chem. Phys.*, 2021, **21**, 13667–13686.

20 N. Illmann, I. Patroescu-Klotz and P. Wiesen, Biomass burning plume chemistry: OH-radical-initiated oxidation of 3-penten-2-one and its main oxidation product 2-hydroxypropanal, *Atmos. Chem. Phys.*, 2021, **21**, 18557–18572.

21 R. Atkinson, Kinetics and mechanisms of the gas-phase reactions of the hydroxyl radical with organic compounds under atmospheric conditions, *Chem. Rev.*, 1986, **86**, 69–201.

22 R. A. Cox, M. Ammann, J. N. Crowley, H. Herrmann, M. E. Jenkin, V. F. McNeill, A. Mellouki, J. Troe and T. J. Wallington, Evaluated kinetic and photochemical data for atmospheric chemistry: Volume VII – Criegee intermediates, *Atmos. Chem. Phys.*, 2020, **20**, 13497–13519.

23 D. J. Stewart, S. H. Almabrok, J. P. Lockhart, O. M. Mohamed, D. R. Nutt, C. Pfrang and G. Marston, *Atmos. Environ.*, 2013, **70**, 227–235.

24 R. Atkinson, J. Arey and E. C. Tuazon, Formation of $O(^3P)$ atoms and epoxides from the gas-phase reaction of O_3 with isoprene, *Res. Chem. Intermed.*, 1994, **20**, 385–394.

 © 2024 The Author(s). Published by the Royal Society of Chemistry

Open Access Article. Published on 19 8 2024. Downloaded on 2026/02/16 5:19:08.
This article is licensed under a Creative Commons Attribution 3.0 Unported Licence.

25 H. E. O'Neal and C. Blumstein, A new mechanism for gas phase ozone–olefin reactions, *Int. J. Chem. Kinet.*, 1973, **5**, 397–413.
26 L. Vereecken, A. Novelli and D. Taraborrelli, Unimolecular decay strongly limits the atmospheric impact of Criegee intermediates, *Phys. Chem. Chem. Phys.*, 2017, **19**, 31599–31612.
27 R. Winterhalter, F. Herrmann, B. Kanawati, T. L. Nguyen, J. Peeters, L. Vereecken and G. K. Moortgat, The gas-phase ozonolysis of of β-caryophyllene ($C_{15}H_{24}$). Part I: an experimental study, *Phys. Chem. Chem. Phys.*, 2009, **11**, 4152–4172.
28 T. L. Nguyen, R. Winterhalter, G. Moortgat, B. Kanawati, J. Peeters and L. Vereecken, The gas-phase ozonolysis of β-caryophyllene ($C_{15}H_{24}$). Part II: A theoretical study, *Phys. Chem. Chem. Phys.*, 2009, **11**, 4173–4183.
29 T. L. Nguyen, J. Peeters and L. Vereecken, Theoretical study of the gas-phase ozonolysis of β-pinene ($C_{10}H_{16}$), *Phys. Chem. Chem. Phys.*, 2009, **11**, 5643–5656.
30 M. E. Jenkin, M. D. Hurley and T. J. Wallington, Investigation of the radical product channel of the $CH_3C(O)O_2$ + HO_2 reaction in the gas phase, *Phys. Chem. Chem. Phys.*, 2007, **9**, 3149–3162.
31 J. D. Crounse, H. C. Knap, K. B. Ørnsø, S. Jørgensen, F. Paulot, H. G. Kjaergaard and P. O. Wennberg, Atmospheric Fate of Methacrolein. 1. Peroxy Radical Isomerization Following Addition of OH and O_2, *J. Phys. Chem. A*, 2012, **116**, 5756–5762.
32 L. Vereecken and B. Nozière, H migration in peroxy radicals under atmospheric conditions, *Atmos. Chem. Phys.*, 2020, **20**, 7429–7458.
33 N. Illmann, I. Patroescu-Klotz and P. Wiesen, Organic acid formation in the gas-phase ozonolysis of α,β-unsaturated ketones, *Phys. Chem. Chem. Phys.*, 2023, **25**, 106–116.
34 R. R. Baldwin and R. W. Walker, Elementary reactions in the oxidation of alkenes, *Symp. Combust. Proc.*, 1981, **18**, 819–829.
35 J. Y. Park, M. C. Heaven and D. Gutman, Kinetics and mechanism of the reaction of vinyl radicals with molecular oxygen, *Chem. Phys. Lett.*, 1984, **104**, 469–474.
36 B. K. Carpenter, Computational prediction of new mechanisms for the reactions of vinyl and phenyl radicals with molecular oxygen, *J. Am. Chem. Soc.*, 1993, **115**, 9806–9807.
37 A. Matsugi and A. Miyoshi, Yield of Formyl Radical from the Vinyl + O_2 Reaction, *Int. J. Chem. Kinet.*, 2014, **46**, 260–274.
38 K. T. Kuwata, L. C. Valin and A. D. Converse, Quantum Chemical and Master Equation Studies of the Methyl Vinyl Carbonyl Oxides Formed in Isoprene Ozonolysis, *J. Phys. Chem. A*, 2005, **109**, 10710–10725.
39 M. J. Newland, C. Mouchel-Vallon, R. Valorso, B. Aumont, L. Vereecken, M. E. Jenkin and A. R. Rickard, Estimation of mechanistic parameters in the gas-phase reactions of ozone with alkenes for use in automated mechanism construction, *Atmos. Chem. Phys.*, 2022, **22**, 6167–6195.
40 M. R. McGillen, Z. T. P. Fried, M. A. H. Khan, K. T. Kuwata, C. M. Martin, S. O'Doherty, F. Pecere, D. E. Shallcross, K. M. Stanley and K. Zhang, Ozonolysis can produce long-lived greenhouse gases from commercial refrigerants, *Proc. Natl. Acad. Sci. U. S. A.*, 2023, **120**, e2312714120.
41 R. Taipale, T. M. Ruuskanen, J. Rinne, M. K. Kajos, H. Hakola, T. Pohja and M. Kulmala, Technical Note: Quantitative long-term measurements of VOC concentrations by PTR-MS – measurement, calibration, and volume mixing ratio calculation methods, *Atmos. Chem. Phys.*, 2008, **8**, 6681–6698.
42 E. Es-sebbar, A. Jolly, Y. Benilan and A. Farooq, Quantitative mid-infrared spectra of allene and propyne from room to high temperatures, *J. Mol. Spectrosc.*, 2014, **305**, 10–16.
43 M. A. H. Khan, K. Lyons, R. Chhantyal-Pun, M. R. McGillen, R. L. Caravan, C. A. Taatjes, A. J. Orr-Ewing, C. J. Percival and D. E. Shallcross, Investigating the Tropospheric Chemistry of Acetic Acid Using the Global 3-D Chemistry Transport Model, STOCHEM-CRI, *J. Geophys. Res.: Atmos.*, 2018, **123**, 6267–6281.